

# Simultaneous reference and differential waveform acquisition in time-resolved terahertz spectroscopy

Krzysztof Iwaszczuk<sup>1</sup>, David G. Cooke<sup>1</sup>, Masazumi Fujiwara<sup>2</sup>, Hideki Hashimoto<sup>2</sup> and Peter Uhd Jepsen<sup>1</sup>

<sup>1</sup>*DTU Fotonik - Department of Photonics Engineering, Technical University of Denmark, DK-2800 Kongens Lyngby, Denmark*

<sup>2</sup>*Department of Physics, Graduate School of Science, Osaka City University, 3-3-138 Sugimoto, Sumiyoshi-ku, Osaka 558-8585, Japan*

[puje@fotonik.dtu.dk](mailto:puje@fotonik.dtu.dk)

**Abstract:** We present a new method for data acquisition in time-resolved terahertz spectroscopy experiments. Our approach is based on simultaneous collection of reference and differential THz scans. Both the optical THz generation beam and the pump beam are modulated at two different frequencies that are not harmonic with respect to each other. Our method allows not only twice as fast data acquisition but also minimization of noise connected to slowly varying laser power fluctuations and timing instabilities. Our use of the nonlinear crystal N-benzyl-2-methyl-4-nitroaniline (BNA) enables time-resolved THz spectroscopy to beyond 5 THz, thereby highlighting that the presented method is especially valuable at higher frequencies where phase errors in the data acquisition become increasingly important.

© 2009 Optical Society of America

**OCIS codes:** (300.6495) Spectroscopy, terahertz; (300.6500) Spectroscopy, time-resolved;

---

## References and links

1. K. P. H. Lui, and F. A. Hegmann, "Ultrafast carrier relaxation in radiation-damaged silicon on sapphire studied by optical-pump-terahertz-probe experiments," *Appl. Phys. Lett.* **78**, 3478 (2001).
2. D. G. Cooke, A. N. MacDonald, A. Hryciw, J. Wang, Q. Li, A. Meldrum, and F. A. Hegmann, "Transient terahertz conductivity in photoexcited silicon nanocrystal films," *Phys. Rev. B* **73**, 193311 (2006).
3. D. G. Cooke, and P. Uhd Jepsen, "Time-resolved THz spectroscopy in a parallel plate waveguide," *Phys. Status Solidi A* **206**, 997, (2009).
4. C. A. Schmuttenmaer, "Exploring Dynamics in the Far-Infrared with Terahertz Spectroscopy," *Chem. Rev.* **104**, 1759 (2004).
5. B. Ferguson, and X.-C. Zhang, "Materials for terahertz science and technology," *Nat. Mater.* **1**, 26 (2002).
6. Z. Jiang, and X.-C. Zhang, "Electro-optic measurement of THz field pulses with a chirped optical beam," *Appl. Phys. Lett.* **72**, 1945 (1998).
7. H. Hashimoto, H. Takahashi, T. Yamada, K. Kuroyanagi, and T. Kobayashi, "Characteristics of the terahertz radiation from single crystals of N-substituted 2-methyl-4-nitroaniline," *J. Phys. Condens. Matter* **13**, L529 (2001).
8. K. Kuroyanagi, M. Fujiwara, H. Hashimoto, H. Takahashi, S. Aoshima, and Y. Tsuchiya, "All Organic Terahertz Electromagnetic Wave Emission and Detection Using Highly Purified N-Benzyl-2-methyl-4-nitroaniline Crystals," *Jpn. J. Appl. Phys.* **45**, 4068 (2006).
9. M. Fujiwara, M. Maruyama, M. Sugisaki, H. Takahashi, S. Aoshima, R. J. Cogdell, and H. Hashimoto, "Determination of the d-Tensor Components of a Single Crystal of N-Benzyl-2-methyl-4-nitroaniline," *Jpn. J. Appl. Phys.* **46**, 1528 (2007).
10. Q. Wu, and X.-C. Zhang, "7 terahertz broadband GaP electro-optic sensor," *Appl. Phys. Lett.* **70**, 1784 (1997).
11. G.L. Dakovski, B. Kubera, S. Lan, and J. Shan, "Finite pump-beam-size effects in optical pump-terahertz probe spectroscopy," *J. Opt. Soc. Am. B* **23**, 139 (2006).

12. M. S. Tyagi, and R. Van Overstraeten, "Minority carrier recombination in heavily-doped silicon," *Solid State Electronics* **26**, 557 (1983).
13. M. C. Beard, G. M. Turner, and C. A. Schmuttenmaer, "Sub-picosecond carrier dynamics in low-temperature grown GaAs as measured by time-resolved THz spectroscopy," *J. Appl. Phys.* **90**, 5915 (2001).
14. S. P. Micken, K.-S. Lee, T.-M. Lu, J. Munch, D. Abbott, and X.-C. Zhang, "Double modulated differential THz-TDS for thin film dielectric characterization," *Microelectr. J.* **33**, 1033 (2002).
15. J. H. Strait, P. A. George, M. Levendorf, M. Blood, F. Rana, and J. Park, "Measurements of the Carrier Dynamics and Terahertz Response of Oriented Germanium Nanowires using Optical-Pump Terahertz-Probe Spectroscopy", *Nano Lett.* **9**, 2967 (2009).
16. M. Beard, G. Turner, and C. Schmuttenmaer, "Transient photoconductivity in GaAs as measured by time-resolved terahertz spectroscopy," *Phys. Rev. B.* **62**, 15764 (2000).
17. M. Schall and P. Uhd Jepsen, "Photoexcited GaAs surfaces studied by transient terahertz time-domain spectroscopy," *Opt. Lett.* **25**, 13 (2000).
18. D. E. Aspnes, and A. A. Studna, "Dielectric functions and optical parameters of Si, Ge, GaP, GaAs, GaSb, InP, InAs, and InSb from 1.5 to 6.0 eV," *Phys. Rev. B* **27**, 985 (1983).
19. F. A. Hegmann, and K. P. H. Lui, "Optical pump-terahertz probe investigation of carrier relaxation in radiation-damaged silicon-on-sapphire," *Proc. of SPIE* **4643**, 31 (2002).

## 1. Introduction

Time-resolved terahertz spectroscopy (TRTS) is a relatively new and powerful experimental technique for studying subpicosecond dynamics of photoexcited charge carriers in semiconductors [1, 2, 3] and other materials [4, 5]. It is a non-contact method capable of determining the evolution of the frequency-dependent photoconductivity with a temporal resolution better than 200 fs. TRTS is a time-domain technique, where the spectral information is obtained by Fourier transform of near-single-cycle transients following interaction with a sample, usually by transmission. To extract the frequency-resolved conductivity of a photoexcited sample, two THz transients are necessary: a reference scan,  $E_{ref}(t)$ , of the unexcited sample and a scan of the pumped sample,  $E_{pump}(t)$ . The most common data acquisition scheme is to separately measure  $E_{ref}(t)$  with a blocked pump beam or at negative pump-probe delay times, and then to measure a differential THz scan,  $\Delta E(t)$ , and calculate  $E_{pump}(t) = E_{ref}(t) + \Delta E(t)$ . In this procedure two scans are taken separately and some false spectral features can be introduced if in between scans the output (power, pulse shape) of the laser system changes. In this paper we present a new method of data acquisition in which both scans are taken simultaneously. This approach is not only twice as fast, but also eliminates spurious errors in the spectroscopy arising from experimental conditions changing during data acquisition.

## 2. Experimental details

Figure 1(a) shows the schematic representation of our time-resolved terahertz spectroscopy setup. A regenerative Ti:sapphire femtosecond laser amplifier was delivering 45 fs, 2.8 mJ pulses with center wavelength of 800 nm at a 1 kHz repetition rate. The laser output was split into three portions: a source beam for THz pulse generation, a pump beam for excitation of the sample and a gating beam for THz detection by free space electro-optic sampling. Terahertz waves were generated by optical rectification in 1.4 mm-thick [010] N-benzyl-2-methyl-4-nitroaniline (BNA) crystal [7, 8]. BNA is an organic nonlinear crystal with high second order nonlinear coefficients [9] and allows a higher bandwidth of generated THz radiation than the most commonly used ZnTe. BNA exhibits a linear dependence of generated electric field versus pump power up to the point when signs of damage are apparent at a fluence of  $\sim 1$  mJ/cm<sup>2</sup>. The 800 nm light transmitted through the BNA crystal is blocked by a black polyethylene sheet, transmissive to the THz pulse. Off-axis parabolic mirrors are used to expand the THz beam and next to collimate and focus it to a  $\sim 1$  mm-diameter spot on the sample. The transmitted THz pulse is then collimated and re-focused onto a [110] GaP crystal (300  $\mu$ m-thick) for free

space electro-optic detection of the THz transients. GaP was chosen for detection over the more efficient ZnTe to allow higher bandwidth detection, as the first phonon is at  $\sim 11$  THz whereas ZnTe has its first phonon at  $\sim 5.3$  THz. [10] The setup was enclosed in a plexiglass box and purged with dry  $N_2$  to avoid water absorption lines. Both the 800 nm probe beam and the pump beam were focused through small holes in the centers of off-axis parabolic mirrors for collinear detection and excitation of the sample at normal incidence. The pump beam was frequency doubled to 400 nm by  $\beta$ -BaB<sub>2</sub>O<sub>4</sub> (BBO) crystal to ensure that the  $\sim 15$  nm penetration depth of the pump beam in semi-insulating gallium arsenide (SI GaAs) creates a thin enough film to fulfil the thin film approximation [19]. The sample was mounted on the back of a 1.5 mm-diameter aperture to aid in pump/probe overlap. The pump beam spot was approximately 3 mm in diameter,  $\sim 3$  times larger than the THz spot which ensured uniform excitation [11]. Two computer controlled delay stages were used to change the pump-probe delay times and also to map the THz pulse shape. The setup was constructed in such a way that one delay stage was scanning the time interval between the pump pulse with respect to both the THz source and probe pulses. In this way the whole THz transient was experiencing a constant delay from the pump pulse [13].

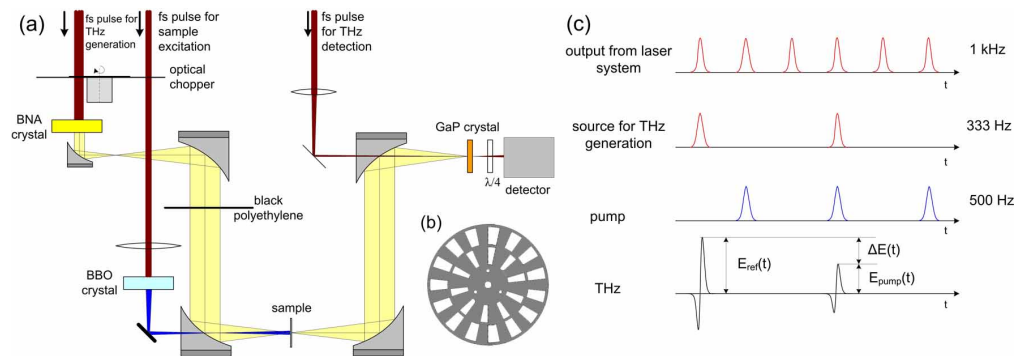


Fig. 1. (a) Schematic of the TRTS setup. (b) 2 frequency chopper blade. (c) time sequence of incoming pulses.

Double modulation is a well-known technique for both static and time-resolved terahertz spectroscopy [14, 15], however to date this has only been used for noise reduction of the differential scan. The key element in simultaneous acquisition of reference and differential THz scans is the use of a two frequency chopper blade, which shape is shown on Fig 1(b). The chopper blade consists of two kinds of sets of slots and shutters. The outer set is built of 15 slots and 15 shutters in equal spacing, while the inner set consists of 10 slots and 10 shutters, where the shutters are twice as wide as the slots. The chopper blade is rotating at such a speed to modulate the beam going through the outer part at 500 Hz, synchronised to the 1-kHz repetition rate of the laser, and at the same time modulate the beam going through the inner part at 333 Hz. The output from the balanced photodiode detector is split and sent to two independent lock-in amplifiers. The reference signals for the lock-in amplifiers are second (500Hz) and third (333 Hz) sub-harmonics of the laser system reference signal, and therefore are not harmonic with respect to each other, so the cross talk between signals measured at those frequencies is on the noise level.

Figure 1(c) shows the time sequence of the laser, pump, generation and THz pulses with respect to each other. The inner chopper blade selects every third pulse which is used for THz generation, while the outer blade transmits every second pulse which is used as a pump. The first

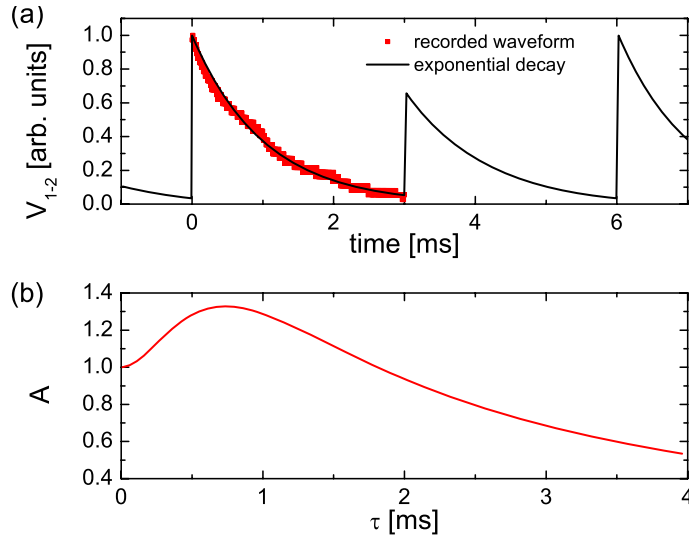


Fig. 2. (a) The experimental waveform (points) of the voltage difference  $V_{1-2}$  between the balanced detector photodiodes with an exponential decay fit (solid line) extended to later times to represent a typical shape of the voltage difference during experiments with the simultaneous data acquisition scheme. The decay constant for the voltage difference was found to be 1.02 ms. (b) The calculated values of the constant  $A$  as a function of photodiodes decay time  $\tau$  under the assumption that voltage difference  $V_{1-2}$  is composed of pure exponential decays.

transmitted THz transient does not experience the presence of a pump, while the transmission of the second THz pulse decreases due to increased absorption from excited free carriers. The reference and pumped electric fields of the terahertz transients can be expressed by the signals measured by the first [ $E_1(t)$ , modulated at 333 Hz] and the second [ $E_2(t)$ , modulated at 500 Hz] lock-in amplifiers by

$$E_{ref}(t) = E_1(t) + AE_2(t) \quad (1)$$

$$E_{pump}(t) = E_1(t) - AE_2(t) \quad (2)$$

where  $A$  is a calibration constant.

Figure 2(a) shows a typical shape of the voltage difference  $V_{1-2}$  between the two balanced photodiodes while monitoring the induced phase retardation at the peak of the THz transient, as illustrated in the lowest row of signals in Fig. 1(c). The exponential decay at  $t = 0$  ms corresponds to the transmitted THz signal strength without pump, whereas the exponential decay at  $t = 3$  ms corresponds to the transmitted THz signal with pump light, thus resulting in a lower amplitude. The values measured by the lock-in amplifiers at 333 Hz and 500 Hz are correspondingly the second ( $a_{333}$ ) and third ( $a_{500}$ ) harmonic Fourier coefficients of the repetitive voltage difference between the two photodiodes with 6-ms period (167 Hz repetition rate). The constant  $A$  can be expressed using  $a_{333}$  and  $a_{500}$  by

$$A = \frac{a_{333}|\text{pump off} - a_{333}|\text{pump on}}{a_{500}|\text{pump on}}. \quad (3)$$

Figure 2(b) shows calculated values of the calibration constant  $A$  as a function of the decay time  $\tau$  of the voltage difference. For fast photodiodes ( $\tau \approx 0$ ) the constant  $A$  is 1, and increases

to a maximum value at  $\tau = 0.75$  ms, followed by a gradual decrease at even slower photodiode response times. We note that not only the decay time constant, but also the detailed shape of the photodiode decay curve can influence the constant  $A$  significantly.

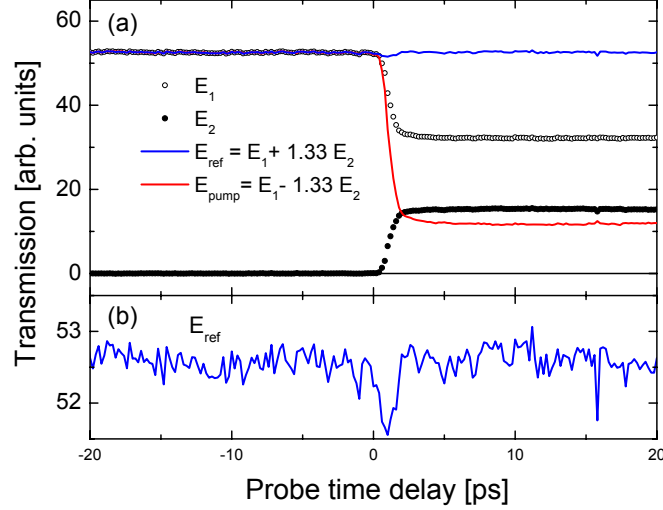


Fig. 3. (a) Measured  $E_1$  and  $E_2$  signals at the peak of THz pulse after 400 nm excitation of semi-insulating silicon in a 1D pump-probe experiment. (b) The recovered reference signal  $E_{ref} = E_1 + AE_2$  ( $A = 1.33$ ) indicating a disordered response at the arrival of the pump.

Figure 3(a) shows the measured  $E_1$  and  $E_2$  signals of the peak of the THz pulse as a function of time after 400 nm excitation of undoped silicon, as well as the calculated  $E_{ref}$  and  $E_{pump}$ . The carrier life time in silicon following 400 nm excitation is on the order of hundreds of  $\mu$ s [12], and so the first 20 ps after excitation the  $E_{pump}$  response is flat. This step-like response allows for accurate experimental determination of the constant  $A$ , which is found to be equal to 1.33. The decay constant of the voltage difference  $V_{1-2}$  between the balanced detector photodiodes was found to be 1.02 ms, what corresponds to the value of  $A$  of 1.28. The difference from the experimentally obtained value can be explained by variations of the voltage difference waveform from a pure exponential decay. Figure 3(b) shows the reference signal  $E_{ref}$ , calculated from  $E_1$  and  $E_2$ .  $E_{ref}$  is constant except near the arrival of the pump where a slight distortion originating from the detector response is visible.

Frequency-resolved THz spectroscopy was performed on a 0.44 mm-thick wafer of semi-insulating gallium arsenide. SI GaAs has become the standard test material for TRTS, for its well known Drude conductivity response [17, 16], carrier dynamics and optical absorption [18]. The complex sheet conductivity  $\Delta\sigma_s = \Delta\sigma'_s + i\Delta\sigma''_s$  of the photoexcited SI GaAs surface can be extracted using the thin film equations [19, 2] :

$$\Delta\sigma'_s(\omega) = \frac{N+1}{Z_0} \left[ \frac{1}{|T(\omega)|} \cos[\Phi(\omega)] - 1 \right] \quad (4)$$

$$\Delta\sigma''_s(\omega) = -\frac{N+1}{Z_0} \left[ \frac{1}{|T(\omega)|} \sin[\Phi(\omega)] \right] \quad (5)$$

where  $N$  is refractive index of the material and  $Z_0$  is the impedance of free space. The amplitude

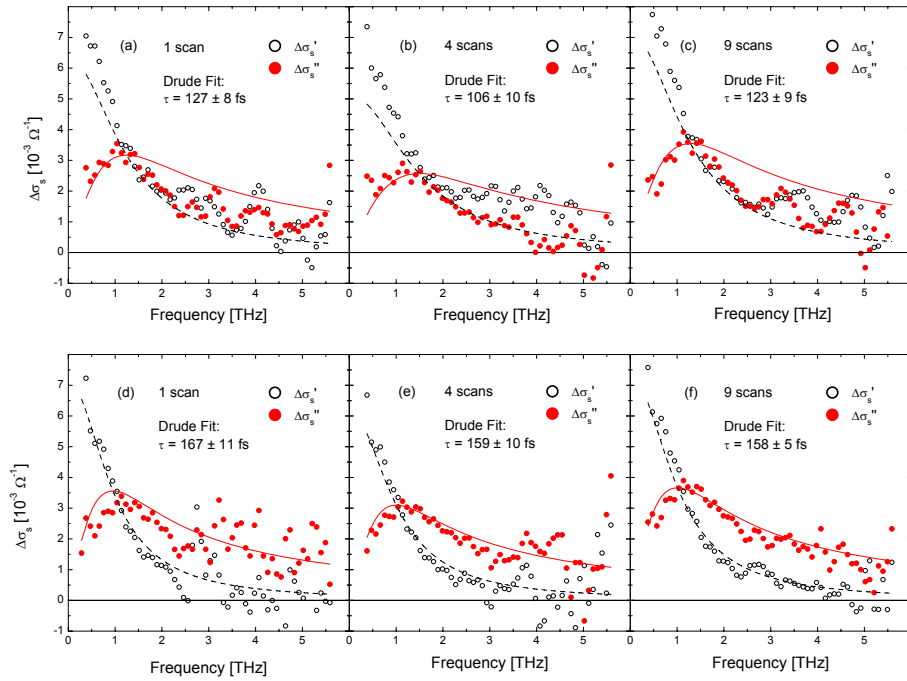


Fig. 4. Complex sheet conductivities  $\Delta\sigma_s = \Delta\sigma'_s + i\Delta\sigma''_s$  of photoexcited SI GaAs, 30 ps after 400 nm excitation at room temperature. Conductivity extracted by taking two separately and (d-f) simultaneously acquired reference and pump waveforms. The lines over the conductivity data are simultaneous Drude fits to  $\Delta\sigma'_s$  and  $\Delta\sigma''_s$  with scattering times given in the figures.

$|T(\omega)| = \frac{|E_{pump}(\omega)|}{|E_{ref}(\omega)|}$  and phase  $\Phi(\omega) = \theta_{pump} - \theta_{ref}$  of the complex transmission function are obtained from the ratio of the Fourier transforms of  $E_{pump}(t)$  and  $E_{ref}(t)$ .

### 3. Results and discussion

Figure 4 presents the complex sheet conductivity,  $\Delta\sigma_s$ , in SI GaAs 30 ps after 400 nm excitation. The applied pump fluence is  $25 \mu\text{J}/\text{cm}^2$  resulting in a maximum differential THz transmission of 21%. The upper row (a-c) shows data obtained with the standard data acquisition method ( $E_{ref}$  and  $\Delta E(t)$  obtained in separate scans), while the lower row (d-f) shows results of measurements in which the simultaneous data collection scheme was applied. The individual plots differ from each other by the number of measured THz pulses used for averaging, which was done in the time domain. The observed transient complex conductivity of photoexcited SI GaAs can be well described by a simple Drude model, although to a varying degree depending on data acquisition method and the number of averaged scans. It is evident that the spectra extracted from the simultaneous detection scheme employed here is better represented by the Drude model than the spectra obtained by separate acquisition. Drude model fits to both  $\Delta\sigma'_s(\omega)$  and  $\Delta\sigma''_s(\omega)$  data were performed simultaneously using the Levenberg-Marquardt algorithm. The Drude scattering time  $\tau$  obtained using the separate and simultaneous acquisition methods differ, and the standard method gives lower values with greater variations. The re-

sults obtained with simultaneous data acquisition are identical within error and the uncertainty decreases with number of scans.

Comparing Fig. 4 (a) and (d) it can be seen that especially at high frequencies the conductivity spectrum obtained using the simultaneous method contains more noise. This behaviour can be explained by the fact that only every third pump pulse is measured by the  $E_2$  signal, so the signal to noise ratio (SNR) decreases by the factor of  $\sqrt{3}$  in comparison to the standard technique. This estimation of SNR is valid under the assumptions that the main source of noise in the system is the laser. In the case when the SNR is determined by the electrical noise from photodiodes and lock-in amplifiers ( $\Delta E$  is not much higher than noise on a base line), the fact that  $E_2 = \frac{1}{2A}\Delta E$  results in further decrease in SNR by the factor of  $2A$ . However, the factor two which is gained in data acquisition speed with the simultaneous method increases signal-to-noise ratio by a factor of  $\sqrt{2}$  for a given acquisition time. This is also observed when comparing Fig. 4(c) and Fig. 4(f). Scatter at high frequencies, caused by the high  $\omega$  roll-off of the THz pulse power spectrum, decreases with number of scans in the average. The bandwidth at which the collected data agrees with the Drude model increases with number of scans only for the simultaneous detection scheme.

Analyzing Figs. 4(a), (b) and (c) we find that data obtained using the standard method are characterized with lower point to point noise, but the agreement with the Drude model is very poor. At frequencies higher than 1.5 THz,  $\Delta\sigma'_s(\omega)$  is higher than expected from the Drude model, while  $\Delta\sigma''_s(\omega)$  is lower than expected. Such a difference can have its origins in a small time shift between the reference  $E_{ref}$  and differential  $\Delta E$  scans. A constant time shift  $\Delta t$  results in a linear phase shift  $\Delta\Phi(\omega) = \omega\Delta t$ . Based on the fact that  $\cos(\Phi + \Delta\Phi) \approx \cos(\Phi) - \Phi\Delta\Phi$  and  $\sin(\Phi + \Delta\Phi) \approx \sin(\Phi) + \Delta\Phi$  (which holds for  $|\Delta\Phi| \ll |\Phi| \ll 1$ ) and using Eqs. 4 and 5 we find expressions for the measured sheet conductivities  $\Delta\sigma'^*_s(\omega)$  and  $\Delta\sigma''^*_s(\omega)$ ,

$$\Delta\sigma'^*_s(\omega) = \Delta\sigma'_s(\omega) - \frac{N+1}{Z_0} \frac{1}{|T(\omega)|} \Phi\Delta\Phi, \quad (6)$$

$$\Delta\sigma''^*_s(\omega) = \Delta\sigma''_s(\omega) - \frac{N+1}{Z_0} \frac{1}{|T(\omega)|} \Delta\Phi. \quad (7)$$

A constant time shift influences both the real and imaginary part of conductivity in a linear fashion with opposite signs of the corrections to the real and the imaginary part ( $\Phi$  is negative for a Drude response). This phase error influences the results of the extracted conductivity more at higher frequencies than lower frequencies. The relative error in the phase will be less in the vicinity of the scattering rate since this is where the transmission function has a peak in its phase response.

An analysis of the data in Fig. 4(c) shows that a constant time shift of 17 fs between the reference and differential scans can explain most of the disagreement between the data and the Drude model. The new value for the scattering time taking this shift into account is  $141 \pm 7$  fs and is in better agreement with that obtained using simultaneous data acquisition scheme. To test the simultaneous data acquisition, we similarly performed a fit including a floating time shift correction to data from figure 4(f). A time shift of  $1.0 \pm 0.5$  fs was found to improve the  $\chi^2$  of the fit, but this is on level of accuracy of delay lines and confirms the principle of simultaneous scans acquisition.

A small time shift between the reference transient  $E_{ref}$  and the differential  $\Delta E$  can have several origins. It can be a result of a change in the optical path between the THz generation and gating pulse (on the order of few just few  $\mu\text{m}$ ), which can be caused by temperature changes of the optical table and elements on it, changes in the refractive index of air due to variations in atmospheric humidity or  $\text{N}_2$  purging conditions, or changes in the output of the laser system. Particularly changes in the near infrared pulse duration can greatly impact the shape of

the amplitude spectrum of the generated THz radiation. Accurate spectroscopy therefore demands very stable laboratory conditions. Because a time shift results in a linear phase shift, this requirement is even more important for high bandwidth spectroscopy. The simultaneous detection scheme presented here eases the demands of these stability conditions. We note that in this case the conductivity response of the tested material was known in advance to be of Drude form. In more exotic materials where the response is unknown, elimination of these artifacts resulting from instability in experimental conditions is imperative for accurate spectroscopy and interpretation of the experimental data.

#### **4. Conclusions**

In summary, we have presented a new method for simultaneous data acquisition in time-resolved terahertz spectroscopy experiments. We have applied this method to extract the sheet conductivity of photoexcited carriers in SI GaAs and compared the results with those of a standard data acquisition scheme. We have shown that application of the new method minimizes errors in spectrally resolved photoconductivity data originating from fluctuations in the laser system output and timing errors in the THz pulse detection.

#### **Acknowledgment**

We are grateful to Danish Defense Acquisition and Logistics Organization and to DTU's H. C. Ørsted fellowship program for financial support.